Computational Geosciences manuscript No.
(will be inserted by the editor)

The role of fluid flow on bone mechanobiology: mathematical modeling and simulation

María Teresa Sánchez · María Ángeles Pérez · José Manuel García-Aznar

Received: date / Accepted: date

Abstract The effect of fluid flow on tissue adaptation was the focus of many research works during the last years. Moreover, the use of poroelasticity models to simulate and understand the interstitial flow movement has taken interest due to the possibility to include the fluid effect on mechanical simulations. In particular, shear stresses induced by bone canalicular fluid flow are suggested to be one of the mechanical stimulus controlling bone remodeling processes. Due to the high difficulty to measure canalicular fluid flow and shear stresses, computational poroelastic models can be used in order to estimate these parameters. In this work, a finite element dual porosity model based on Russian doll poroelasticity is developed. Two experiments with a turkey ulna and a human femur are simulated. Bone lacuno-canalicular fluid flow is computed and compared with the experimental results, focusing on the zones of bone remodeling and showing a relation between this flow and the bone formation process.

Keywords Poroelasticity · Interstitial fluid flow · Nested porosity · Bone remodeling · Cortical bone

M.T. Sánchez
Centro Universitario de la Defensa de Zaragoza. Zaragoza 50090, Spain.
Instituto Universitario de investigación en Matemáticas y Aplicaciones (IUMA), Universidad de Zaragoza. Zaragoza, Spain. Tel.: +34976739853
Fax: +34976739824
E-mail: tererua@unizar.es

M.A. Pérez, J.M. García-Aznar
M2BE-Multiscale in Mechanical and Biological Engineering, Instituto de Investigación en Ingeniería de Aragón (I3A), Instituto de Investigación Sanitaria Aragón (IIS Aragón), Universidad de Zaragoza, Zaragoza, Spain.

1 Introduction

Bone is a living material whose main function is forming the skeleton and therefore enabling locomotion and protection of the organism. In consequence, it is subjected to permanent and transient loads caused by daily activity or specific events such as accidents. It is well-known that bones adapt their properties depending on the loads they are supporting and respond differently to them, exhibiting thus an heterogeneous behavior [12]. Furthermore, bone can be considered as a porous material formed by a mixture of components where water is transporting nutrients and waste products [17].

Bone is structured with a hierarchical network of porosities with quite different characteristic dimensions [8]. Vascular porosity (PV) contains blood vessels and nerves and it is associated with blood irrigation of the bone. The lacuno-canalicular porosity (PLC) is the network where the osteocytes are embedded and collagen-apatite porosity (PCA) is associated with the spaces between collagen and mineral in the bone matrix. These three porosities are nested hierarchically one inside the other and the typical pore size is 50 μm for the vascular porosity, 100 nm for the lacunar-canalicular one, and 1 nm for the collagen-apatite one. All of these porosities are filled with bone fluid, but in PCA the fluid flow is negligible [8]. Due to that, the focus on studying the bone fluid flow lies on the PV and PLC porosities and the ratio between their pore sizes is approximately 167 [11]. Furthermore, there exist some differences between the PLC and the PV porosities: the bone fluid in the PLC can sustain higher pressure for longer time due to mechanical loading whereas PV will function as a low-pressure reservoir that interchanges bone fluid with the PLC. The mechanical loads applied to the whole bone moves the bone fluid in the PLC. In compression, the

bone fluid moves from the PLC to the PV, and in tension, this fluid is sucked from the PV to the PLC. This process of draining and absorption greatly affects the fluid pressure in the PLC while hardly affects to the pressure in the PV. These differences in pressure are directly related to the fact that the linear dimension associated with the PV is two orders of magnitude larger than the associated with the PLC.

Bone has also the ability of adapting its structure to the mechanical environment in a process known as bone remodeling [27]. The specific mechanical stimulus controlling this process is not completely understood [9], but evidences suggest that it is related with lacunocanalicular fluid flow and the shear stresses that exerts to the osteocytes [26,9,3,14]. However, measuring fluid flow velocities and shear stresses in the lacunocanalicular network is difficult [4] and different computational models have been developed to estimate these quantities [23,6,24,19,25,16,1,13,2,18,21,20]. In most of these models, bone fluid flow was studied microscopically, simulating a small portion of bone and using poroelasticity models to calculate the PLC fluid flow. Steck *et al.* [24] was the first work with a macroscopic approach although they only considered the lacunocanalicular porosity and not the vascular porosity. Later, Fornells *et al.* [13] applied a dual porosity poroelastic model to compute fluid flow in both PV and PLC, but this macroscopic model was not able to analyze the fluid flow at the level of an osteon. More recently, Cowin and Cardoso [7] and Cardoso *et al.* [10] gathered different analytical and numerical models to understand the influence of the fluid interchange between the bone porosities in the bone tissue mechanotransduction. They reviewed a model for poroelastic materials with hierarchical pore space architecture for the description of interstitial fluid flow in bone, that was firstly introduced in [11,15], the Russian doll poroelastic model. In [11], Cowin *et al.* obtained an analytical solution to the interchange of pore fluid between the PV and the PLC in bone tissue due to cyclic mechanical loading and Gailani and Cowin [15] used this model to determine this interchange due to a ramp loading.

The objective of this work is to simulate numerically the behavior of the fluid flow in the cortical bone taking into account the hierarchical relation between the PV and PLC porosities. Considering the porous structure of bone and the almost independent behaviour of the fluid pressure in the vascular and lacuno-canalicular domains (see [8,11]), we will propose to simulate this process by considering two separate continuum poroelastic models to represent each level of porosity. The coupling between the two models, consisting of the fluid flow between them, occurs through sources connecting the PV and PLC porosities. The Russian doll poroelastic model [11] is employed to computationally model the bone fluid flow at PV and at the level of an osteon at the PLC. Then, a finite element (FE) simulation is carried out to compute the different flows and their influence in several factors related with bone remodeling. Two different simulations have been developed to test this model considering two experiments: the application of a loading regime to maintain bone mass in a turkey ulna [22], and the influence of age on the osteon size of a human femur [5].

2 Methods

The Russian doll porosity formulation used in this work was proposed by Cowin *et al.* [11], where they presented a particular pore space structure model to simulate the interstitial pore fluid flow in tissues like bone, tendon, meniscus, etc. This model is called Russian doll poroelastic model since it recalls a nested set of Russian dolls: the different porosities are nested within the other and a porosity with a specific pore size can only drain its fluid into a porosity with a smaller pore size, and receive it from a porosity with a larger pore size (or viceversa). This model is based on considering each porosity level as a separate poroelastic continuum problem, with interaction between them through source and sink terms that allow the transfer of fluid on the boundaries.

Here, we are going to implement the Russian doll model in a FE approach to simulate the influence of the fluid flow in the bone response under different mechanical loads.

2.1 Mathematical model

The mathematical model of the cortical bone consists of two poroelastic formulations to solve and compute the deformations, stresses and pressures for each porosity (PV and PLC) with a coupling term between them in order to take into account their fluid interchange. Fig. 1 shows an scheme of the considered cortical bone that is formed by several osteons connected to each other. In the figure, a particular osteon is highlighted. An osteon is a roughly hollow cylindrical structure with 0.2 mm of radius. The PLC porosity lies in the annular domain of the osteon whereas the PV porosity corresponds to the central section of the bone. The connection between the two porosities takes place in the inner cylindrical wall of the different osteons (the hollow part of the osteon belongs to the PV domain).

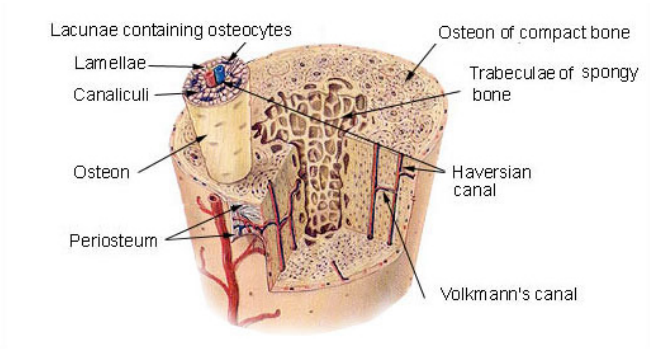

Fig. 1 Diagram of a typical long bone showing one of the osteons. Both the section of the long bone and the osteon can be modeled as hollow cylinders. The osteon is part of the PLC porosity whereas its inner lumen is part of the PV porosity. Courtesy of SEER - U.S. National Cancer Institute's Surveillance, Epidemiology and End Results (SEER) Program.

2.1.1 Poroelastic model for PV

The quasi-static equilibrium of the bone is governed by the mechanical equilibrium equation

$$\mathrm{div}(\boldsymbol{\sigma}_v) + \mathbf{F}_v = \mathbf{0}, \tag{1}$$

where $\boldsymbol{\sigma}_v$ denotes the total stress tensor and $\mathbf{F}_v$ are the external volume forces.

Bone is assumed to be a poroelastic material and therefore, the constitutive law relating the stress tensor $\boldsymbol{\sigma}_v$ with the suffered deformation $\boldsymbol{\varepsilon}(\mathbf{u}_v)$ and the pore fluid pressure p_v is as follows:

$$\boldsymbol{\sigma}_v = \lambda_v \mathrm{tr}(\boldsymbol{\varepsilon}(\mathbf{u}_v))\mathbb{1} + \mu_v \boldsymbol{\varepsilon}(\mathbf{u}_v) - \alpha_v p_v \mathbb{1}, \tag{2}$$

where $\mathbf{u}_v$ denotes the displacement field, λ_v and μ_v are the Lamé coefficients related with the Young's modulus and the Poisson's ratio through the usual expressions, respectively, and α_v is the Biot effective stress coefficient; $\mathbb{1}$ denotes the identity tensor.

The governing equation for the fluid flow in the PV is obtained from the mass conservation equation for the fluid. First, Darcy's law describes the fluid flow through the porous medium conformed by the bone structure, that is,

$$\mathbf{q}_v = -\frac{\boldsymbol{\kappa}_v}{\eta_v}\nabla p_v, \tag{3}$$
$$\mathbf{q}_v = \phi_v\left(\mathbf{v}_f - \dot{\mathbf{u}}_v\right), \quad \dot{\mathbf{u}}_v = \frac{\partial \mathbf{u}_v}{\partial t},$$

where $\mathbf{q}_v$ is the percolation velocity, given in terms of the fluid velocity $\mathbf{v}_f$ and the solid velocity $\dot{\mathbf{u}}_v$, ϕ_v is the porosity of the medium, $\boldsymbol{\kappa}_v$ is the permeability tensor of the bone, and η_v the fluid viscosity. In general, the definition of the permeability tensor $\boldsymbol{\kappa}$ depends on the isotropic or anisotropic properties of the material. Here, we consider the isotropic and orthotropic cases:

$$\boldsymbol{\kappa} = \begin{cases} \kappa\mathbb{1} & \text{for the isotropic case,} \\ \begin{pmatrix} \kappa_{11} & 0 & 0 \\ 0 & \kappa_{22} & 0 \\ 0 & 0 & \kappa_{33} \end{pmatrix} & \text{for the orthotropic case.} \end{cases}$$

Second, we consider the mass balance equation for the solid phase, taking into account the fluid content variation, that is:

$$\frac{1}{M_v}\frac{\partial p_v}{\partial t} + \mathrm{div}(\mathbf{q}_v) + \frac{\partial}{\partial t}\mathrm{tr}\left(\alpha_v \boldsymbol{\varepsilon}(\mathbf{u}_v)\right) = -\Gamma, \tag{4}$$

where M_v is the Biot modulus or constrained specific storage coefficient given by the expression

$$\frac{1}{M_v} = \frac{\phi_v}{K_f^v} - \frac{\alpha_v - \phi_v}{K_s^v},$$

being K_f^v and K_s^v are the bulk modulus of fluid and solid part, respectively. In Eq. 4, Γ corresponds to the leakage term that takes into account the rate of flow between canaliculi and Haversian canals, i.e., the fluid interchange between the PV and PLC porosities. This term can be written as follows:

$$\Gamma = \gamma(p_v - p_l), \tag{5}$$

where p_v is the pore pressure in the PV porosity, p_l the pore pressure in the PLC and γ is the leakage parameter.

Gathering Eqs. 1-5, the proposed system of differential equations is the following:

$$\begin{aligned} \mathrm{div}(\boldsymbol{\sigma}_v) + \mathbf{F}_v &= \mathbf{0}, \\ \boldsymbol{\sigma}_v = \lambda_v \mathrm{tr}(\boldsymbol{\varepsilon}(\mathbf{u}))\mathbb{1} + \mu_v \boldsymbol{\varepsilon}(\mathbf{u}) - \alpha_v p_v \mathbb{1}&, \\ \frac{1}{M_v}\frac{\partial p_v}{\partial t} - \boldsymbol{\kappa}_v \nabla^2 p_v + \frac{\partial}{\partial t}\mathrm{tr}\left(\alpha_v \boldsymbol{\varepsilon}(\mathbf{u})\right) &= -\gamma(p_v - p_l). \end{aligned}$$

Boundary conditions for the vascular porosity PV are medullary pressure in the endosteum (taking it as reference pressure, so $p_m = 0$) and no fluid flow across the periosteum. Displacement boundary conditions depend on the characteristics of each specific simulation.

2.1.2 Poroelastic model for PLC

In the lacuno-canalicular porosity, the system of differential equations is similar to that proposed for the PV, that is,

$$\begin{aligned} \mathrm{div}(\boldsymbol{\sigma}_l) + \mathbf{F}_l &= \mathbf{0}, \\ \boldsymbol{\sigma}_l = \lambda_l \mathrm{tr}(\boldsymbol{\varepsilon}(\mathbf{u}_l))\mathbb{1} + \mu_l \boldsymbol{\varepsilon}(\mathbf{u}_l) - \alpha_l p_l \mathbb{1}&, \\ \frac{1}{M_l}\frac{\partial p_l}{\partial t} - \boldsymbol{\kappa}_l \nabla^2 p_l + \frac{\partial}{\partial t}\mathrm{tr}\left(\alpha_l \boldsymbol{\varepsilon}(\mathbf{u}_l)\right) &= \gamma(p_v - p_l), \end{aligned}$$

where $\mathbf{u}_l$ and $\boldsymbol{\sigma}_l$ are the displacement field and stress tensor suffered by the osteon material in the lacuno-canalicular porosity and p_l is the corresponding pore fluid pressure.

Boundary conditions for the lacuno-canalicular porosity PLC are fluid flow not allowed through the cement line and pressure in the Haversian canal equal to the obtained with the vascular model PV. In this case, displacement boundary conditions are also derived from the vascular model.

2.2 Numerical implementation

Regarding the numerical solution, the simulations at bone scale and at osteon scale are solved separately, that is, the problems for the PV and PLC are solved in an uncoupled way. This simplification can be made due to the different orders of magnitude between the PV and PLC fluid pressures and porosities. Although the two porosities exchange fluids (the fluid transport occurs through sources connecting the two different porosity levels), the influence on the fluid pressure is small, and the two poroelastic problems could solve independently. Thus, the resulting matrix systems are:

– for the vascular model:

$$\boldsymbol{K}u_v^N - \alpha_v \boldsymbol{C}p_v^N = \boldsymbol{R}_v^N,$$
$$\alpha_v \boldsymbol{C}^t \dot{u}_v^N + (\boldsymbol{H}_v + \gamma\mathbf{M})\, p_v^N + \frac{1}{M_v}\boldsymbol{M}\dot{p}_v^N = \boldsymbol{Q}_v^N + \gamma\mathbf{M}p_l^N,$$

– for the lacuno-canalicular model:

$$\boldsymbol{K}u_l^N - \alpha_l \boldsymbol{C}p_l^N = \boldsymbol{R}_l^N,$$
$$\alpha_l \boldsymbol{C}^t \dot{u}_l^N + (\boldsymbol{H}_l + \gamma\mathbf{M})\, p_l^N + \frac{1}{M_l}\boldsymbol{M}\dot{p}_l^N = \boldsymbol{Q}_l^N + \gamma\mathbf{M}p_v^N,$$

where the superscript N denotes the time step. The matrices used in the previous systems are the following:

$$\boldsymbol{K} = \int_V \boldsymbol{B}_u^T \boldsymbol{D}\boldsymbol{B}_u \mathrm{d}V,$$
$$\boldsymbol{H}_n = \int_V \boldsymbol{B}_p^T \boldsymbol{K}_n \mathbf{B}_p \mathrm{d}V, \quad n \in \{v, l\},$$
$$\boldsymbol{R}_n = \int_V \boldsymbol{N}^T \boldsymbol{F}_n \mathrm{d}V + \int_S \boldsymbol{N}^T \boldsymbol{T}\mathrm{d}S,$$
$$\boldsymbol{Q}_n = \int_S \boldsymbol{N}^T \boldsymbol{q}_n \mathrm{d}S,$$
$$\boldsymbol{C} = \int_V \boldsymbol{B}_u \boldsymbol{N}\mathrm{d}V, \quad \boldsymbol{M} = \int_V \boldsymbol{N}^T\boldsymbol{N}\mathrm{d}V,$$

where $\boldsymbol{N}$ is the matrix of shape functions corresponding to the discretization of the problem, $\boldsymbol{B_u}$ and $\boldsymbol{B_p}$ are the deformation matrices written in terms of the derivatives of shape functions, $\boldsymbol{D}$ corresponds to the constitutive stress-strain matrix, $\boldsymbol{K}_v$ and $\boldsymbol{K}_l$ represent the permeability matrices for the PV and PLC porosities, respectively; $\boldsymbol{F}_n$ corresponds to the external volume load vector, $\boldsymbol{T}$ is the external surface load vector and $\boldsymbol{q}_n$ the fluid flux vector for the PV and PLC porosities. Displacements and pressures are approached by means of linear shape functions and a backward Euler scheme is used to compute the unknowns at each time step.

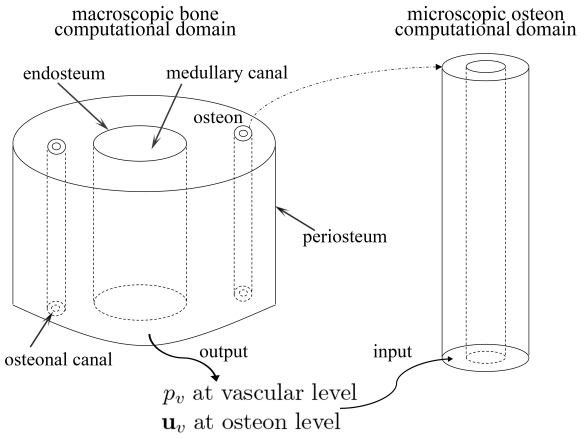

Fig. 2 Scheme of the two computational domains of interest.

The numerical simulation of the two problems is carried out by using the FE commercial code Abaqus (Dassault Systems, Suresnes, France) and it was implemented as user element routines. Fig. 2 shows a scheme of the two computational domains considered for this numerical simulation. Firstly, the macroscopic model at bone level is solved and the obtained results, that is, the displacements on the nodes and pressures on the elements, are used as boundary conditions to simulate the problem at osteon scale in different osteons placed in different locations. To do that, two different meshes are considered: a macroscopic mesh to discretize the domain corresponding to the bone section and a microscopic mesh to represent the different osteons simulated in the bone section. The coupling between these two scales and meshes is implemented by using linear interpolation in the displacement and pressure fields and assuming that the elements of the considered osteon are located in the geometrical center of certain elements of the macroscopic bone section.

3 Results

In order to validate the applicability and potential of the Russian doll poroelastic model, several mechanical load conditions were simulated by considering two real applications to compute the effective fluid flow in bone: the morphometric change in a turkey ulna [22] and the influence of the osteon size in the fluid flow in a human femur [5].

Table 1 Parameter values of the turkey ulna Russian doll poroelastic model.

Young Modulus E	15.8 GPa
Poisson's ratio ν	0.3
Vascular porosity ϕ_v	0.04
Orthotropic vascular permeability k_{11}	10^{-13} m^2
Orthotropic vascular permeability k_{22}	10^{-13} m^2
Orthotropic vascular permeability k_{33}	10^{-12} m^2
Lacuno-canalicular porosity ϕ_l	0.05
Lacuno-canalicular permeability k_l	10^{-20} m^2

3.1 Changes in bone morphology in a turkey ulna experiment

We first simulated the experimental work of Qin *et al.* [22], where they determined the ability of a relative high-frequency and moderate-duration loading regime to maintain bone mass in a turkey ulna model of disuse osteopenia. A bending load was applied to a small sample of bone to determine the morphometric change of bone at the mid-diaphysis.

A section of the turkey ulna was modeled with the following geometrical dimensions: 6 mm of height, 10 mm of small external diameter, 16 mm of big external diameter and approximately 1.7 mm of cortical thickness (see Fig. 3). Sinusoidal mechanical loading of 30 Hz was applied and the specimen was subjected to a bending load of 9 N through compression at the dorsal side (see Fig.3(a)). The section of the turkey ulna is composed of 15444 nodes and 12285 elements.

Six bone sectors were considered (see Fig. 3(b)); an osteon is assumed in each sector where the morphometric bone change will be analyzed. Each osteon is modeled as a cylinder of 200 μm of length, 15 μm of internal diameter and 76 μm of external diameter. Its finite element model consists of 9360 nodes and 8200 elements (see Fig. 3(c)).

The cortical bone of the turkey ulna section is assumed to be an elastic material with a Young's modulus of 15.8 GPa and a Poisson's ratio of 0.3; however, its poroelastic properties are assumed to be orthotropic. Regarding the osteon, it is also assumed to be an elastic material but with isotropic poroelastic properties. The values of the properties of the turkey ulna used in the simulation are detailed in Table 1 (see [13,25,28]).

With this model, we analyze the effective pore fluid velocity at the level of an osteon and we try to relate it with the morphometric change of bone at the mid-diaphysis determined experimentally in [22].

Fig. 4 gathers the effective fluid flow on the six osteons considered in the bone section. The maximum fluid flow is reached at osteons 2 and 5 with a coincident value. These sectors correspond to the higher morphometric changes of bone determined experimentally in [22], where the mechanical loading resulted in a significative reduction of bone loss when compared to the results obtained in disuse. Moreover, the minimum value for the fluid flow is obtained at osteons 3 and 6, being also the sector where more bone loss was observed in the experiments. These results allow us to infer a relation between the effective fluid flow in the osteons and the bone adaptation processes: the greater the fluid flow in the osteon, the lower bone loss is obtained.

3.2 Relation between the human femoral osteon size and age with the fluid flow

In this section we infer a relationship between the fluid flow and the osteon size, taking into account the analysis carried out by Britz *et al.* [5], where they evaluated the impact of age, sex and body size in human femoral osteon geometry, concluding that decreasing the osteon size with age was the dominant pattern of variation. By using the Russian doll poroelastic model to simulate those experiments, we aim to find a relation between the effective fluid flow on osteons with changes in the corresponding osteon size.

With this objective in mind, we consider a section of a human femur to which a bending load of sinusoidal type is applied (see Fig. 5(a)). The effective fluid flows at the three osteons located at the femur shown in Fig. 5(b) are analyzed. The osteons are modeled as hollow cylinders (see Fig. 5(c)) with two different diameters, 250 μm corresponding to a 20 years old specimen and 201 μm corresponding to a 90 years old specimen. The internal diameter is of 15 μm and the length of 200 μm.

The computational mesh of the section of the human femur is composed of 11772 nodes and 9878 elements whereas the computational mesh for the osteon model consists of 13754 nodes and 12125 elements (see Fig. 5(c)).

Similarly to the previous experiment, both the cortical bone and the osteon are assumed to be elastic materials but with orthotropic poroelastic properties

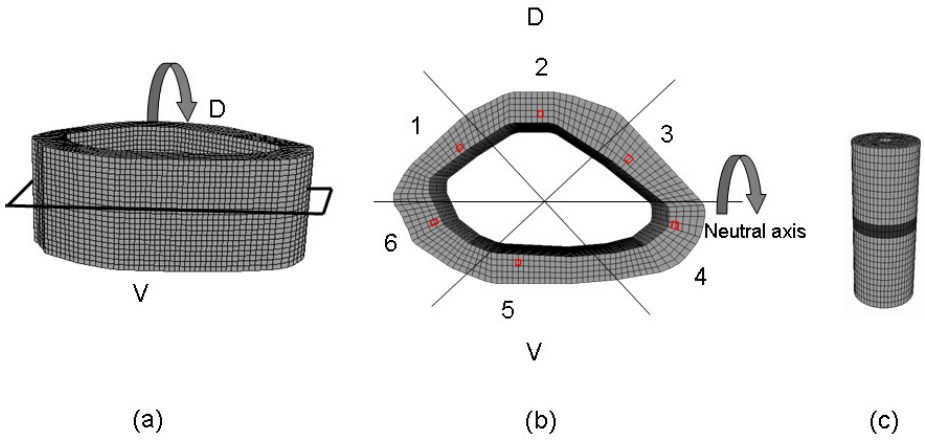

Fig. 3 (a) Finite element model of the turkey ulna section under a bending load (D = dorsal and V = ventral); (b) cross section of the finite element model showing the neutral axis when subjected to the bending load with the six osteons (bold points marked) considered at each bone sector; (c) finite element model of the osteons.

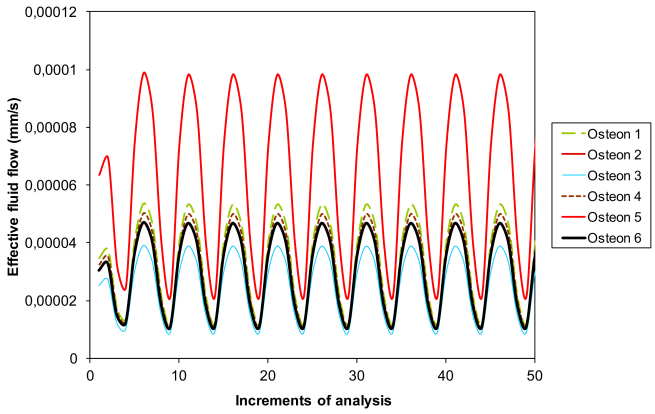

Fig. 4 Effective fluid flow at PLC on the six osteons.

Table 2 Parameter values of the human femur Russian doll poroelastic model.

Young Modulus E	15.8 GPa
Poisson's ratio ν	0.3
Vascular porosity ϕ_v	0.04
Orthotropic vascular permeability k_{11}	10^{-14} m^2
Orthotropic vascular permeability k_{22}	10^{-14} m^2
Orthotropic vascular permeability k_{33}	10^{-13} m^2
Lacuno-canalicular porosity ϕ_l	0.05
Lacuno-canalicular permeability k_l	1.7×10^{-20} m^2

in the case of the cortical bone and isotropic properties for the osteon. The values of the properties of the human femur used in this simulation are detailed in Table 2 (see [13]).

Fig. 6 shows the effective fluid flow at three different osteons for the two different sizes. Notice that the application of the same force at the macroscopic bone produces a clear reduction of the effective fluid flow for the young specimen (250 μm) in the three osteons.

Fig. 7 shows the reaction forces in the macroscopic analysis for the two diameters of the osteon corresponding to the reference load. With the aim to obtain the same effective fluid flow for the two different osteon sizes, a reduction in the force applied in the osteon of 201 μm (old specimen) is needed. In this way, after carrying out the microscopic analysis, a significant reduction in the fluid flow for the osteon size of 201 μm is obtained and as a consequence, it coincides with the values corresponding to the osteon size of 250 μm. Fig. 8 gathers the results obtained for the reference forces with the two osteon sizes and for the lower force for the old specimen.

The obtained results allow us to infer that, since old people reduce their activity (there exists a load reduction in the loads at the femur), in order to have the same effective fluid flow at the osteon level, the osteon diameter should be reduced.

4 Conclusions

In this work we have presented the application of the Russian doll poroelastic model developed by Cowin and co-authors [11,15] to compute and analyze the effect of the fluid flow in the vascular and lacuno-canalicular porosities with the objective to determine its influence in the bone adaptation processes. The proposed model takes into account the two different bone porous networks by considering a combination of macroscopic and microscopic approaches for the two levels. This allows to compute numerically and enhance the evaluation of fluid flows and pressures of both PV and PLC porosities. Moreover, the proposed model also permits the computation of the fluid flow at osteon level and the

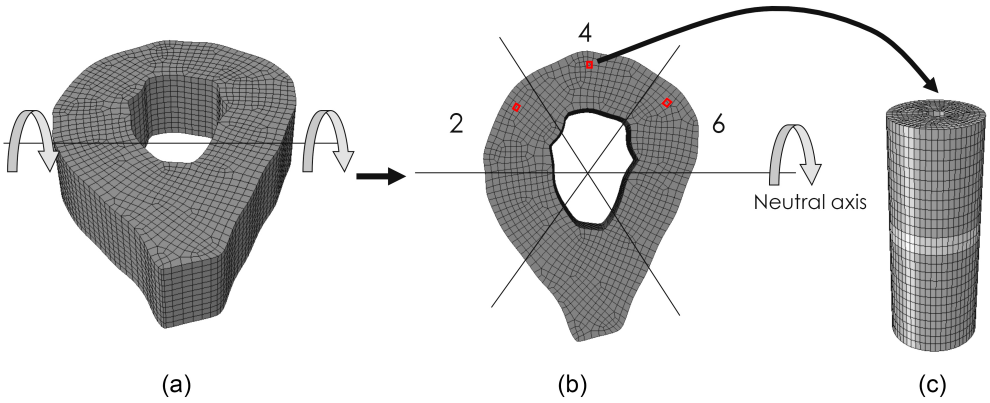

Fig. 5 (a) Finite element model of the human femur section under a bending load; (b) cross section of the finite element model showing the neutral axis when subjected to the bending load with the three osteons (bold points marked) considered at each bone sector; (c) finite element model of the osteons located in previous femur section.

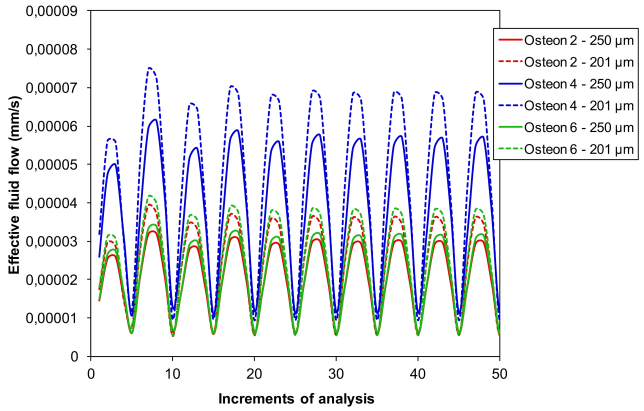

Fig. 6 Effective fluid flow through three different osteons for the two osteon sizes. A reduction in the fluid velocity is produced in the young specimen for the same applied load.

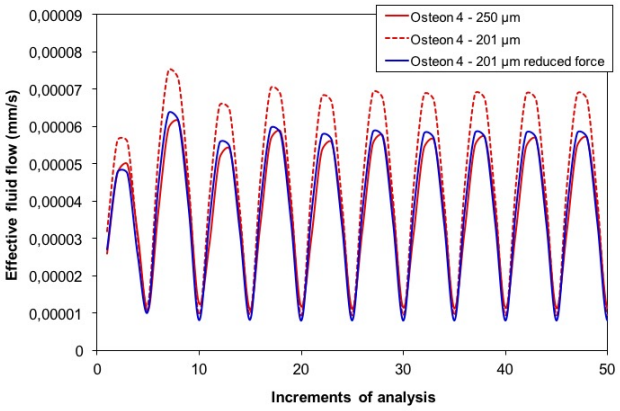

Fig. 8 Comparison of effective fluid flow through osteon 4 with two different applied forces. When a low force is applied, the fluid flow corresponding to the old specimen is closer to the young one.

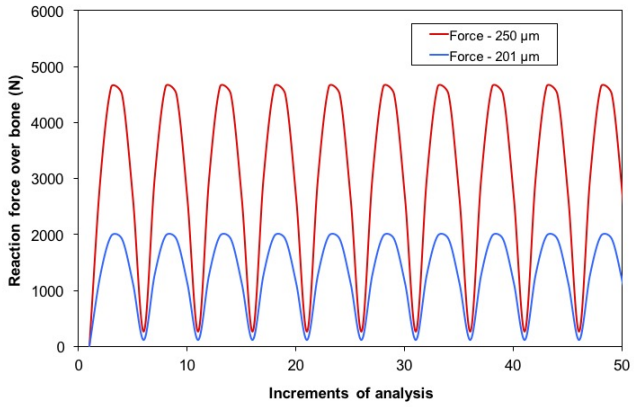

Fig. 7 Reaction forces obtained in the bone for two different values of the osteon size.

consequent analysis of its influence in different experiments.

In order to check the potential of the Russian doll poroelastic model, we have carried out a numerical simulation of the experiment by Qin *et al.* [22], which consists of the application of a relative high-frequency and moderate-duration loading regime to a section of a turkey ulna. The objective of this experiment was to determine the bone sector where the bone loss is reduced. The results obtained with the model presented here have shown the same behaviour that those obtained experimentally.

Moreover, we have used the Russian doll poroelastic model to infer a relation between the fluid flow and the osteon size, and relate this with age following the analysis given in [5]. To do that, we have carried out a numerical simulation of a section of a human femur subjected to a bending load of sinusoidal type. The obtained results let computationally determine that a reduction of activity (generally, in old people) implies a

reduction of the osteon diameter in order to have the same effective fluid flow at the osteon level.

Nevertheless, the proposed model presents some limitations. Although an orthotropic behavior was assumed for the vascular porosity, a more realistic model at microstructure level should be considered. Moreover, the osteon geometries in both examples were assumed with the same type and size although they represent different species. This was due to the absence of information regarding the experimental data. In a future study more realistic data and different osteon geometries would be analysed.

Summarizing, the finite element model based on Russian doll poroelasticity has been able to demonstrate that the lacuno-canalicular fluid flow is one of the main stimulus to regulate adaptive bone response. Furthermore, the application of this model to other examples could provide a more detailed assessment of the intracortical remodeling process during human bone development.

Acknowledgements The authors gratefully acknowledge the support from the Spanish Ministry of Economy and Competitiveness through research projects DPI2015-64221-C2-1-R, DPI2017-84780-C2-1-R and RTI2018-094494-B-C21.

References

1. Anderson, E.J., Kaliyamoorthy, S., Alexander, J.I.D., Knothe Tate, M.L.: Nano-microscale models of periosteocytic flow show differences in stresses imparted to cell body processes. Ann. Biomed. Eng. **33**, 52–62 (2005)
2. Anderson, E.J., Knothe Tate, M.L.: Idealization of pericellular fluid space geometry and dimension results in a profound underprediction of nano-microscale stresses imparted by fluid drag on osteocytes. J. Biomech. **41**, 1736–1746 (2008)
3. Bacabac, R.G., Smit, T.H., Mullender, M.G., Van Loon, J.J.W.A., Klein-Nulend, J.: Initial stress-kick is required for fluid shear stress-induced rate dependent activation bone cells. I. Ann. Biomed. Eng. **33**, 104–110 (2005)
4. Beno, T., Yoon, Y., Cowin, S.C., Fritton, S.P.: Estimation of bone permeability using accurate microstructural measurements. J. Biomech. **39**, 2378–2387 (2006)
5. Britz, H.M., Thomas, C.D.L., Clement, J.G., Cooper, D.M.: The relation of femoral osteon geometry to age, sex, height and weight. Bone **45**(1), 77 – 83 (2009)
6. Burger, E.H., Klein-Nulend, J., Smit, T.H.: Strain-derived canalicular fluid flow regulates osteoclast activity in a remodelling osteon - a proposal. J. Biomech. **36**, 1453–1459 (2003)
7. Cardoso, L., Fritton, S.P., Gailani, G., Benalla, M., Cowin, S.C.: Advances in assessment of bone porosity, permeability and interstitial fluid flow. J. Biomech. **46**(2), 253 – 265 (2013)
8. Cowin, S.: Bone poroelasticity. J. Biomech. **32**, 217–238 (1999)
9. Cowin, S.: Mechanosensation and fluid transport in living bone. J. Muskuloske Neuron. Interact. **2**, 256–260 (2002)
10. Cowin, S.C., Cardoso, L.: Blood and interstitial flow in the hierarchical pore space architecture of bone tissue. J. Biomech. **48**(5), 842 – 854 (2015)
11. Cowin, S.C., Gailani, G., Benalla, M.: Hierarchical poroelasticity: movement of interstitial fluid between porosity levels in bones. Philos. Trans. Royal Soc. A **367**(1902), 3401–3444 (2009)
12. Cowin, S.C., Hegedus, D.H.: Bone remodeling i: theory of adaptive elasticity. J. Elast. **6**(3), 313–326 (1976)
13. Fornells, P., García-Aznar, J.M., Doblaré, M.: A finite element dual porosity approach to model deformation-induced fluid flow in cortical bone. Ann. Biomed. Eng. **35**, 1687–1698 (2007)
14. Fritton, S.P., Weinbaum, S.: Fluid and solute transport in bone: Flow-induced mechanotransduction. Annu. Rev. Fluid Mech. **41**(1), 347–374 (2009)
15. Gailani, G., Cowin, S.: Ramp loading in russian doll poroelasticity. J. Mech. Phys. Solids **59**(1), 103 – 120 (2011)
16. Gururaja, S., Kim, H.J., Swan, C.C., Brand, R.A., Lakes, R.S.: Modeling deformation-induced fluid flow in cortical bone's canalicular-lacunar system. Ann. Biomed. Eng. **33**, 7–25 (2005)
17. Harrigan, T.P., Hamilton, J.J.: Bone strain sensation via transmembrane potential changes in surface osteoblasts: Loading rate and microstructural implications. J. Biomech. **26**(2), 183 – 200 (1993)
18. Kumar, N.C., Dantzig, J., Jasiuk, I.: Modeling of cortical bone adaptation in a rat ulna: Effect of frequency. Bone **50**(3), 792 – 797 (2012)
19. Mak, A.F.T., Huang, D.T., Zhang, J.D., Tong, P.: Deformation induced hierarchical flows and drag forces in bone canaliculi and matrix microporosity. J. Biomech. **30**, 11–18 (1997)
20. Pereira, A.F., Javaheri, B., Pitsillides, A.A., Shefelbine, S.J.: Predicting cortical bone adaptation to axial loading in the mouse tibia. J. Royal Soc. Interface **12**(110), 20150590 (2015)
21. Pereira, A.F., Shefelbine, S.J.: The influence of load repetition in bone mechanotransduction using poroelastic finite-element models: the impact of permeability. Biomech. Model. Mechanobiol. **13**(1), 215–225 (2014)
22. Qin, Y., Rubin, C.T., McLeod, K.J.: Nonlinear dependence of loading intensity and cycle number in the maintenance of bone mass and morphology. J. Orthop. Res. **16**, 482–489 (1998)
23. Smit, T.H., Burger, E.H., Huyghe, J.M.: A case for strain-induced fluid flow as regulator of bmu-coupling and osteonal alignment. J. Bone Miner. Res. **17**, 2021–2029 (2002)
24. Steck, R., Niederer, P., Knothe Tate, M.L.: A finite element analysis for the prediction of load-induced fluid flow and mechanochemical transduction in bone. J. Theor. Biol. **220**, 249–259 (2003)
25. Wang, L., Fritton, S.P., Cowin, S.C., Weinbaum, S.: Fluid pressure relaxation depends upon osteon microstructure: modelling an oscillatory bending experiment. J. Biomech. **32**, 663–672 (1999)
26. Weinbaum, S., Cowin, S., Zeng, Y.: A model for the excitation of osteocytes by mechanical loading-induced bone fluid shear stresses. J. Biomech. **27**(3), 339 – 360 (1994)
27. Wolff, J.: Das gesetz der transformation der knochen. Hirschwald, Berlin (1892)
28. Zhang, D., Weinbaum, S., Cowin, S.C.: Estimates of the peak pressures in bone pore water. J. Biomech. Eng. **120**, 697–703 (1998)